

## Alkali-halide cluster ions produced by laser vaporization of solids

Y. J. Twu, C. W. S. Conover, Y. A. Yang, and L. A. Bloomfield  
*Department of Physics, University of Virginia, Charlottesville, Virginia 22901*  
 (Received 15 February 1990; revised manuscript received 4 May 1990)

The mass spectra of alkali-halide cluster ions  $M(MX)_n^+$  and  $X(MX)_n^-$ , produced by laser vaporization of a solid sample, were measured by tilted-plate time-of-flight mass spectrometry. The measured abundances of sodium chloride clusters ( $n = 1-200$ ), sodium iodide clusters ( $n = 1-125$ ), cesium chloride clusters ( $n = 1-125$ ), and cesium iodide clusters ( $n = 1-100$ ) confirm that surface terraces are the most stable additions to a cuboid base lattice. Also, the spectra show that the relative stabilities of certain cluster ions are dependent on the ionic radii of the constituent atoms.

### I. INTRODUCTION

Alkali-halide clusters have been widely studied because they are easily formed and because their ionic natures permit simple but reliable calculations of their binding energies. They also serve an important role in our understanding of the connections between molecule and crystal. The properties of an alkali-halide molecule and the corresponding crystal are quite different. For example, a NaCl monomer has an interatomic distance of about 2.36 Å, a binding energy of 5.75 eV, and a vibrational frequency of  $336 \text{ cm}^{-1}$ ,<sup>1</sup> while a NaCl crystal has a lattice constant of 2.82 Å, a lattice energy of 7.92 eV/molecule, and a vibrational frequency of  $170 \text{ cm}^{-1}$ .<sup>2</sup> The lattice energy is much higher than the binding energy of the monomers even though the molecule has a much smaller bond length and a much higher vibrational frequency. By studying alkali-halide clusters we can provide information about how crystals grow and how crystalline properties evolve.

Particle sputtering, inert-gas condensation, and laser vaporization have all been used to produce clusters of alkali halides.<sup>3-5</sup> The mass spectra of clusters generated by these three techniques all show some degree of contrast between abundant and rare cluster sizes, indicating a high degree of order within these small particles. Unfortunately, mass selection and determination are possible only if a cluster is charged. Thus, the simplest species to study are those with an excess positive or negative charge. Alkali-halide cluster ions observed in mass spectrometers usually contain many more nonstoichiometric clusters than those with equal numbers of alkali-metal and halogen atoms. This fact is due to the ionic nature of the binding within the alkali-halide solids. If an electron is added to or removed from a cluster composed of equal numbers of alkali-metal positive ions and halide negative ions  $(MX)_{n+1}$ , that electron or hole will neutralize one of the ions. The resulting neutral atom is bound to the remaining ions  $M(MX)_n^+$  or  $X(MX)_n^-$  through a relatively weak monopole-induced-dipole interaction and is easily removed at thermal energies.<sup>6</sup>

In the work described in this paper, we used a tilted-plate time-of-flight mass spectrometer<sup>7</sup> to measure the

abundances of alkali-halide cluster ions produced by a laser vaporization cluster source. Specifically, we have determined the abundances of sodium chloride, sodium iodide, cesium iodide, and cesium chloride clusters, in order to make comparisons between the abundance spectra of clusters with different binding energies and ratios of the ionic radii of their constituent atoms. Furthermore, sodium chloride and sodium iodide crystallize into the sixfold-coordinated fcc rock-salt structure and cesium chloride and cesium iodide prefer an eightfold-coordinated bcc lattice structure at normal pressures and temperatures. In spite of this difference, we observe that the cluster mass spectra of those alkali halides are all surprisingly similar, except for some unique features of  $I(\text{NaI})_n^-$  clusters.

Finally, we have observed mass spectra of cluster ions extending beyond 27 000 amu [ $\text{Cs}(\text{CsI})_n^+$  with  $n > 100$ ]. Larger particles are almost certainly present, but it is not possible to detect them with conventional detectors.

### II. EXPERIMENTAL DETAILS

An overview of the experimental apparatus is shown in Fig. 1. The main chamber contains a pulsed laser-vaporization supersonic nozzle source. A laser is used to vaporize the surface of a solid alkali-halide salt to produce clusters which are then entrained and cooled by a freely expanding supersonic jet of helium gas. The clusters are carried downstream and are collimated with a conical skimmer. They enter a tilted-plate time-of-flight mass spectrometer in which a square high-voltage pulse is used to accelerate charged clusters horizontally. Because clusters with different masses acquire different velocities during the acceleration, the amount of time it takes for the clusters to arrive at the end of the time-of-flight region depends upon their masses. A dual microchannel plate detector is placed at the end of the flight region to register the cluster ion arrivals. Data collection is entirely under computer control so that a complete mass spectrum can be taken for each laser pulse.

We studied four alkali-halide compounds, NaCl, NaI, CsCl, and CsI, and also looked at the spectra for KCl. We chose Na, Cl, Cs, and I in order to determine the

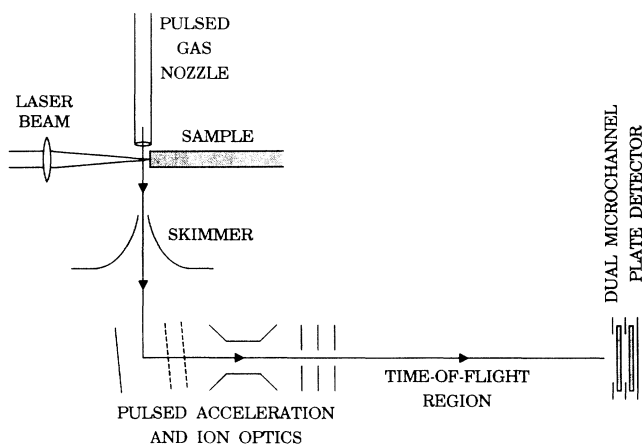


FIG. 1. Experimental apparatus: Cluster ions are produced by laser vaporization of the sample and are cooled and entrained in a helium-gas jet. The mass spectra of clusters produced in the source are obtained by tilted-plate time-of-flight mass spectrometry.

dependence of the spectra on the binding energy and ionic sizes of the constituents. These four atoms mark the most extreme sizes of alkali-metal and halogen elements that we could study. We also tried LiF and CsF as source samples but were unable to generate good pulses of clusters of these materials with our apparatus. The binding energies and band gaps of these compounds are probably too high for the vaporization process. For example, the binding energy of a lithium fluoride crystal is about 10.5 eV/molecule with a band gap of more than 12 eV.<sup>2</sup> The laser beam is unable to vaporize the crystal effectively. Instead, it only breaks the crystal into macroscopic pieces. The mass spectra only covered  $n = 1-22$  for lithium fluoride and  $n = 1-40$  for cesium fluoride.

In the source, a laser is used to vaporize the surface of a solid alkali-halide salt (powdered sample or single crystal) into a freely expanding supersonic jet of helium gas. Two different lasers were used to vaporize the samples. One is a Lambda Physik EMG103MSC excimer laser, operating with ArF at 193 nm, with 80–200 mJ in each 17-ns pulse. This beam is focused to a spot about 1 mm  $\times$  2 mm, for an energy density of about 4–10 J/cm<sup>2</sup>. The second laser is a Spectra-Physics DCR-3A neodymium-doped yttrium aluminum garnet (Nd:YAG) laser, operated at the second or fourth harmonic with a nominal infrared pulse length of either 8 or 2 ns. The energy of 532 nm is 50–100 mJ and at 266 nm is 5–10 mJ, yielding energy densities on the sample of about 100–200 J/cm<sup>2</sup> at 532 nm and about 10–20 J/cm<sup>2</sup> at 266 nm. The higher-energy densities necessary at longer wavelengths reflect the multiphoton processes that are responsible for the vaporization process and cluster generation. The ideal vaporization wavelengths fall in the range where one photon is transmitted but two photons are absorbed.

Two sodium chloride source samples were used in pre-

vious studies with this apparatus.<sup>5</sup> One is sodium chloride single crystal, another is a packed powder source, sodium chloride powder between two stainless-steel disks. It was found that the mass spectra are not dependent upon whether a single crystal or a powder sample is used in a laser-vaporization cluster source. In this work, we used both configurations for different materials, but the independence of the spectra to sample preparation allows us to compare the results.

For two materials, NaI and CsCl, we packed a powder between two 3-in.-diam stainless-steel disks and added a small amount of distilled deionized water to the powder to make the sample more rigid. The samples were then placed in vacuum, where the water was removed by evaporation. For the other materials, NaCl, CsCl, and KCl, 2.0-in.-diam single-crystal disks were used. Inserted at the focus of the laser, these disks were rotated at about 5 revolutions per minute to keep the laser from drilling deep irregular holes in the sample. Rotation also made the entire edge of the sample available for producing clusters.

A 165–205- $\mu$ s pulse of helium gas at 10–12 bars pressure passes across the sample during the laser-vaporization process. These gas pulses are produced by a Lasertechnics LPV valve with a 1.00-mm orifice and are directed across the sample through a 1.25-mm-i.d. cylindrical nozzle. The gas begins to undergo a supersonic free-jet expansion just above the edge of the sample disk, passing across the thin edge of the sample before expanding into the vacuum. The focused laser beam hits the sample about 1 mm below the nozzle opening, so that vaporized particles are cooled and entrained in the gas and thus also undergo supersonic expansion. The gas emitted by this nozzle has a substantial effect on the pressure in the source vacuum chamber and limits the repetition rate of the apparatus to approximately 50 pulses per second. The average pressure in the source vacuum chamber is typically  $(2-5) \times 10^{-5}$  Torr when the gas pulse is on at 10 Hz and  $2 \times 10^{-6}$  Torr otherwise.

The laser-generated hot alkali-halide particles undergo very rapid cooling upon entering the gas. Immediately after leaving the solid surface, the distribution of cluster energies and sizes are approximately random, and the high-temperature clusters evaporate atoms, molecules, and ions at a rapid rate. This decay, if allowed to proceed, would continue until the clusters did not have enough energy to evaporate off any more particles. Thus the end states of those particles are not necessarily the most stable ones, but rather the end states occur when the daughter particles have run out of energy for further decay. Therefore, a random distribution of initial energies leads to a primarily random final distribution of cluster sizes, though more stable clusters would tend to be marginally more common than unstable ones.

In our experiment, decay proceeds until the cooling gas removes enough energy to prevent further decay. Also, the rapid decrease in density and temperature during the jet expansion ensures that each particle suffers less than 1% of the collisions needed for observing significant cluster growth in a laser-vaporization cluster source.<sup>8</sup> Experiments using mixed alkali-halide powder targets have

shown that virtually no growth takes place following vaporization.<sup>9</sup> Therefore, the final distribution of clusters is determined by the cluster abundances at the time of cooling. In an evolving group of clusters, those cluster sizes that live the longest are the most likely to be seen at any given time.<sup>10</sup> So the enhanced populations in the mass spectra correspond to those sizes that exist longest at high temperature before decaying into smaller particles. The final abundances of clusters essentially reflect their high-temperature stabilities against decay.<sup>5</sup>

Despite having enough energy to induce evaporative decays on nanosecond time scales, the clusters are evidently ordered during the time when their high-temperature stabilities are being tested. If they were fully liquid, there would be little structure to the observed abundance spectra. The ordered particles evaporate away weakly bound molecules and the size distribution evolves from smooth to highly structured during the final nanoseconds before the helium gas stops all decay. Clusters produced by secondary-ion mass spectrometry (SIMS) have been shown to evolve from a random size distribution immediately after sputtering,<sup>11</sup> to a highly structured size distribution microseconds later.<sup>12</sup> The SIMS experiments using a double-focusing magnetic mass spectrometer resemble the present work in that they are most sensitive to clusters that do not decay during their flight through the spectrometer. They observe similar contrasts between abundant and rare cluster sizes.<sup>12</sup>

In addition to cooling the clusters, the helium-gas pulse entrains the clusters and cluster ions, carrying them through the supersonic expansion and accelerating them to the velocity of the helium atoms. The resulting beam of helium gas and small particles is skimmed 15 cm downstream from the source by a Beam Dynamics conical skimmer with a 2.0-mm-diam orifice. The clusters and cluster ions then enter the acceleration region of the tilted-plate time-of-flight mass spectrometer.

A laser-vaporization cluster source produces an intense pulse of clusters. Time-of-flight mass spectrometry is well suited to the pulsed structure of the beam, since the technique disperses the clusters in time so that one time-resolved ion detector can record the entire spectrum of masses in a single pulse. As shown in Fig. 1, the cluster beam goes vertically down to the accelerating region of the tilted-plate time-of-flight mass spectrometer (TOFMS), transverse to the spectrometer's horizontal flight path. Since all of the particles arrive at the acceleration region with the same initial velocity, the thermal velocity of the helium gas, heavier particles enter the region with larger kinetic energies. For high Mach numbers (significantly supersonic), the velocity is  $v \approx (5k_B T_0/m_{\text{He}})^{1/2}$ , where  $T_0$  is the temperature of the high-pressure helium before expansion,  $m_{\text{He}}$  is the mass of a helium atom, and  $k_B$  is Boltzmann's constant.<sup>13</sup> Thus, for a cluster with mass 5000 amu, the initial kinetic energy can be as high as 100 eV. This large, mass-dependent initial energy complicates mass spectrometry used to analyze the species present in the beam. To compensate for this initial velocity, different kinds of time-of-flight mass spectrometers were designed, as shown in Fig. 2.

The most basic design, Fig. 2(a), just accelerates particles toward the detector and cannot take into account kinetic energy differences due to differences in initial position between the plates. This problem was compensated for in a three-plate acceleration scheme, Fig. 2(b), introduced in 1951 by Wiley and McLaren,<sup>14</sup> which focuses particles of the same mass in time at the detector, but still does not approach the initial energy problem. The standard solution to the initial energy problem is to place deflection plates just after the acceleration plates, as in Fig. 2(c). For a given choice of deflection voltage, we can have a certain range of cluster masses directed at the detector. However, this scheme is inadequate for very heavy clusters. For example, when our 10-kV TOFMS is configured in this manner, clusters of more than 6000 amu collide with the deflection plates and cannot be detected. Our solution, Fig. 2(d), is to tilt the acceleration plates so that part of the impulse a particle receives when the acceleration field is on goes into removing its transverse velocity.<sup>7</sup>

In this manner, we can compensate for a cluster's high initial kinetic energy and direct the ion beam down the axis of the spectrometer. We are also able to focus the beam in time and in space more easily because the axial nature of the ion beam in the spectrometer allows an ad-

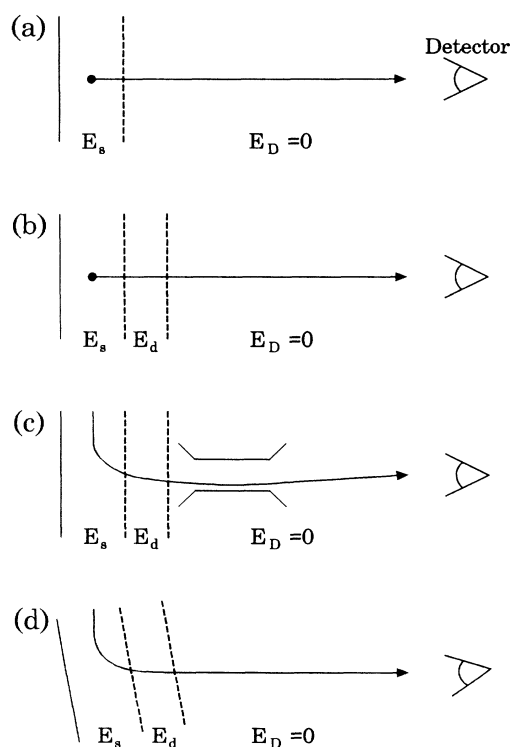


FIG. 2. Four types of time-of-flight mass spectrometers: (a) single-field mass spectrometer, (b) two-field (Wiley-McLaren) mass spectrometer, (c) two-field mass spectrometer with deflection plates to correct for initial particle velocity, and (d) tilted-plate time-of-flight mass spectrometer, which also corrects for initial particle velocity.

ditional axial ion lens to produce a spatially well-focused ion beam at the detector. The tilt angle that exactly cancels a cluster's initial velocity is mass dependent, but the spectrometer is effective for a considerable range of masses around the optimum. Furthermore, the upper mass limit of our spectrometer is much higher than in the fixed-plate designs. However, because the three-plate acceleration scheme achieves time focusing in a plane parallel to the accelerating plates, the detector should also be tilted at the same angle as the plates. Our apparatus does not presently permit tilting the detector to match the tilted accelerating plates, resulting in a slight reduction in resolution.

In this work, we have used a combination of both the deflection plates and the tilted-plate time-of-flight mass spectrometer (Fig. 1). With the plates tilted at an angle  $\theta$  optimized for a particular mass, the cluster ions close to that mass leave the acceleration region along the axis of the flight path with a velocity approximately proportional to the inverse square root of their mass. Once accelerated, the cluster ions enter the deflection region and a small deflection field steers the clusters directly towards the detector.

The tilted-plate accelerating region consists of three parallel stainless-steel plates (10 cm  $\times$  10 cm  $\times$  0.08 cm), bolted together with nylon screws and ceramic insulators so that the three plates form a rigid, independent structure. The first accelerating region is 2.54 cm wide and the second region is 1.27 cm wide. Ions can pass from one accelerating region to the next through oblong holes (1.59 cm  $\times$  2.54 cm) machined in the centers of the stainless-steel plates. These holes are covered by fine copper grids (Buckbee-Mears MC-17, 70 lines/in.) which are held in place with high-vacuum silver paint. To tilt the plates, we support the accelerating assembly with a Teflon arm and horizontal stainless-steel support rod so that the axis of the support rod is centered on the first acceleration region. A 360° precision rotation stage permits the rod and plate assembly to rotate about the center of the first accelerating region. The oblong holes in the accelerating plates are longest in the vertical direction, to compensate for the foreshortening that occurs when the plates are rotated.

Each cycle, after the pulse of clusters has freely drifted into the accelerating region, we turn on the accelerating fields. The accelerating voltage, 8.8–10.0 kV, is produced by a Velonex model 350 high-power, high-voltage pulse generator with a pulse transformer. The Velonex pulse generator is powered through a constant voltage transformer to increase its voltage stability. Our choice of the accelerating region sizes requires the relation between the electric field in the first region ( $E_1$ ) and the second region ( $E_2$ ) to be  $E_1 \approx 0.068E_2$  for time focusing. The majority of the acceleration is thus done in the second region. The rise time of the high-voltage pulse is approximately 400 ns. The lightest clusters move significantly while the field is being turned on and so receive less than the full  $\sim 10$  keV of energy available. This imperfection in the acceleration process complicates the relationship between velocity and mass, but is a minor inconvenience that is easily overcome during data analysis.

After acceleration, the clusters traverse a flight path 150 cm in length, which begins with the electrostatic deflection region. This deflection region contains two pairs of plates, 7.5 cm wide, 5 cm long, and spaced 1.25 cm apart. The vertical deflection plates are placed 4 cm after the accelerating plates and are followed 1.25 cm later by the horizontal deflection plates. These plates provide minor steering corrections to direct the clusters toward the detector. The vertical plates operate at between 0 and 200 V, depending on the mass of the clusters being studied and the tilt angle of the acceleration field. The horizontal plates operate in the range  $\pm 5$  V. A three-plate einzel lens follows the deflection plates, but is unnecessary for these experiments.

At the end of the flight region, there is a 1.8-cm-diam dual-microchannel-plate detector (Galileo MCM-18-B) to register the arrivals of the cluster ions. The detection efficiency of the microchannel plate falls off dramatically at particle velocities below  $1.5 \times 10^4$  m/s.<sup>15</sup> Thus at 10 keV total kinetic energy, the detector becomes relatively inefficient at detecting particles of more than 12 000 amu. However, because we are primarily interested in the relative abundances of clusters of nearby masses, this efficiency drop for large clusters is not a severe limitation. The current signal from the microchannel-plate detector is amplified, when necessary, and digitized for analysis by a computer.

Because a given setting of the acceleration region tilt and deflection plate voltage directs only about a 20% mass range toward the detector, the overall cluster mass spectra had to be pieced together from many small segments. Each segment was optimized for a specific mass range. Between 200 and 1200 cycles of the apparatus were averaged to produce each segment of the spectrum. The number of clusters produced at a particular cluster size was then determined by integrating the digitized current signal produced by that cluster's arrival at the detector. Using only the central few cluster peaks from a given segment, the entire mass spectra were pieced together by scaling each segment until the values of cluster populations common to two adjacent segments agreed. The piecing-together process certainly introduced some cumulative error between clusters of widely different mass. However, because we are primarily interested in the relative abundances of nearby clusters, that overall error is unimportant.

The laser-vaporization supersonic nozzle source and the tilted-plate time-of-flight mass spectrometer work very well together. The mass resolution of the accelerating system and time-of-flight mass spectrometer is observed to be 1 part in 500, as predicted in a previous work.<sup>5</sup> In Figs. 3(a) and 3(b) we show the current signals produced by clusters with the largest number of atoms,  $\text{Cl}(\text{NaCl})_{203}^-$  (407 atoms), and by the heaviest clusters,  $\text{Cs}(\text{CsI})_{102}^+$  ( $\sim 26$  500 amu), we have measured. Without tilting the plates, the simple deflection plates design fails to work for clusters larger than  $\text{Cs}(\text{CsI})_{23}^+$  ( $\sim 6000$  amu).<sup>7</sup>

Using this technique, we have obtained spectra for the nonstoichiometric clusters,  $M(\text{MX})_n^+$  and  $X(\text{MX})_n^-$ , of sodium chloride ( $n = 1-200$ ), sodium iodide

( $n = 1-125$ ), cesium chloride ( $n = 1-125$ ), and cesium iodide ( $n = 1-100$ ). The mass resolution for each material is about 1 part in 500, 1 part in 400, 1 part in 400, and 1 part in 350, respectively. This decrease in resolution with increasing cluster mass is largely due to two factors. First, the cluster beam is not perfectly collimated when it enters the acceleration region and there is nothing in the spectrometer that can compensate for transverse initial velocity in the cluster. The heavier the cluster, the more transverse velocity affects resolution. Second, we did not tilt the detector to match the tilted accelerating plates. For the 1.8-cm-diam dual-microchannel plate, with the accelerating field tilted  $5^\circ$ , the flight-time differences between particles hitting different parts of the detector can exceed 0.1% of the overall flight time. The heavier particles require larger tilt angles, increasing the flight-time differences and reducing resolution.

### III. MASS SPECTRA OF ALKALI-HALIDE CLUSTER IONS

As discussed in the preceding section, the final abundances of clusters from a laser-vaporization supersonic

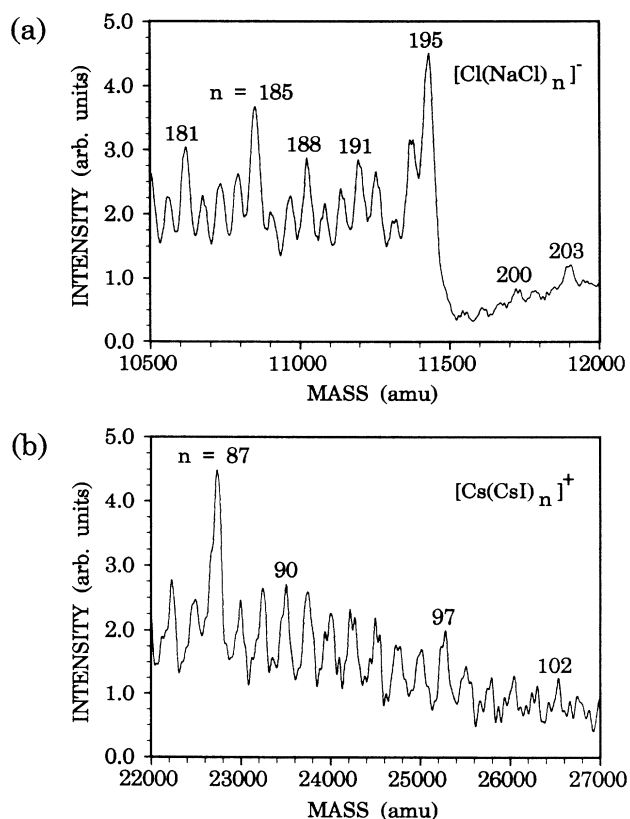


FIG. 3. (a) Mass spectrum of negative sodium chloride cluster ions produced by laser vaporization. Mass resolution is 1 part in 500 when isotopic effects have been included. (b) Mass spectrum of positive cesium iodide cluster ions. Both traces show the raw charged particle signal displayed against arrival time, converted into atomic mass units.

nozzle source reflect their high-temperature stabilities against decay. A cluster stops decaying when the cooling gas removes most of its excess energy, and because this cooling occurs quickly, the final distribution of cluster masses is determined by the cluster abundances at the time of cooling. The longer a particular cluster size can withstand the decay due to excess energy, the more such clusters will be frozen into the gas jet.

Unfortunately, there are four additional processes that can affect abundances even after the clusters have cooled and stopped decaying. Electron attachment, charge exchange, photoionization, and photofragmentation can complicate the mass spectra if they occur after the cooling has occurred. The first three processes change the charge state of the clusters so that a cluster that is particularly stable with one charge state may appear abundant in other charge states as well. These charge-changing processes often neutralize one of the ions within the cluster, allowing it to evaporate even at relatively low energy.

The fourth process, photofragmentation, is the decay of clusters due to reheating by the laser beam. As long as the photoabsorption cross section is either very small or nearly uniform for nearby clusters, such absorption will only delay the cooling process. We expect it to have little effect on the abundance measurements. It is also interesting that the spectra are remarkably insensitive to experimental parameters such as sample geometry, laser fluence, wavelength, or pulse length, and measurement time delays. It is possible to misadjust the equipment so as to stop producing clusters altogether or to reduce the production of heavy clusters somewhat. However, the relative abundances of adjacent cluster sizes is only very slightly affected.

The relative cluster ion abundances vary dramatically with the number of atoms in the clusters. By far the most abundant sizes are those that form a complete cuboid lattice, a tiny complete fcc salt crystal. The next most abundant group of clusters consists of those clusters that contain full surface terraces, built on the face of a complete cuboid base lattice. While these two groups of clusters appear unusually abundant regardless of which alkali or halogen ions are involved, the contrasts between different cluster sizes depend on the binding energies and effective radii of the constituent ions.

#### A. Sodium chloride clusters

Spectra of the nonstoichiometric sodium chloride cluster ions  $\text{Na}(\text{NaCl})_n^+$  and  $\text{Cl}(\text{NaCl})_n^-$  appear in Fig. 4. Particularly abundant are the cluster ions at  $n = 4, 13, 22, 37, 62, 87, 122,$  and  $171$ , corresponding to the particularly stable cuboid ionic arrangements of  $3 \text{ ions} \times 3 \text{ ions} \times 1 \text{ ion}$ ,  $3 \times 3 \times 3$ ,  $3 \times 3 \times 5$ ,  $3 \times 5 \times 5$ ,  $5 \times 5 \times 5$ ,  $5 \times 5 \times 7$ ,  $5 \times 7 \times 7$ , and  $7 \times 7 \times 7$ , respectively, and consistent with previous studies.<sup>3,16</sup> For example,  $n = 13$  has 27 ions and forms a  $3 \times 3 \times 3$ -ion cube. Other cuboid abundance peaks occur at  $n = 31, 52, 67, 112, 115,$  and  $157$  and correspond to cuboids of  $3 \times 3 \times 7$ ,  $3 \times 5 \times 7$ ,  $3 \times 5 \times 9$ ,  $5 \times 5 \times 9$ ,  $3 \times 7 \times 11$ , and  $5 \times 7 \times 9$  ions. Furthermore, the low abundances of the cluster ions immediately following those stable  $n$  values indicate instabilities of the

ions or lack of an energy barrier barring the removal of one or two sodium chloride molecules from the energetically stable structures.

There is also an additional fine structure, particularly evident in the positive clusters, which we attribute to surface terraces built upon complete cuboid lattices.<sup>17,5</sup> For example, consider the  $3 \times 5 \times 5$  cuboid  $n = 37$  as shown in Fig. 5. If one row of three NaCl molecules is removed, the relatively abundant  $n = 34$  is obtained. If a second row of three molecules is removed, we have the abundant  $n = 31$ , and so on, all the way to  $n = 13$ , which is a  $3 \times 3 \times 3$  cube. The abundance of every third cluster size in this range is enhanced. Above  $n = 37$ ,  $3 \times 3 \times 5$ , surface terraces containing five molecules ( $\delta n = 5$ ) are also present in the spectra, becoming the dominant sequence above  $n = 52$ . This  $\delta n = 5$  periodicity continues until  $n = 122$ , where  $\delta n = 7$  surface terraces become dominant.

The presence of these features, cuboid fcc microcrystalline lattices and complete surface terraces on those lattices, is a good indication that the binding in these sys-

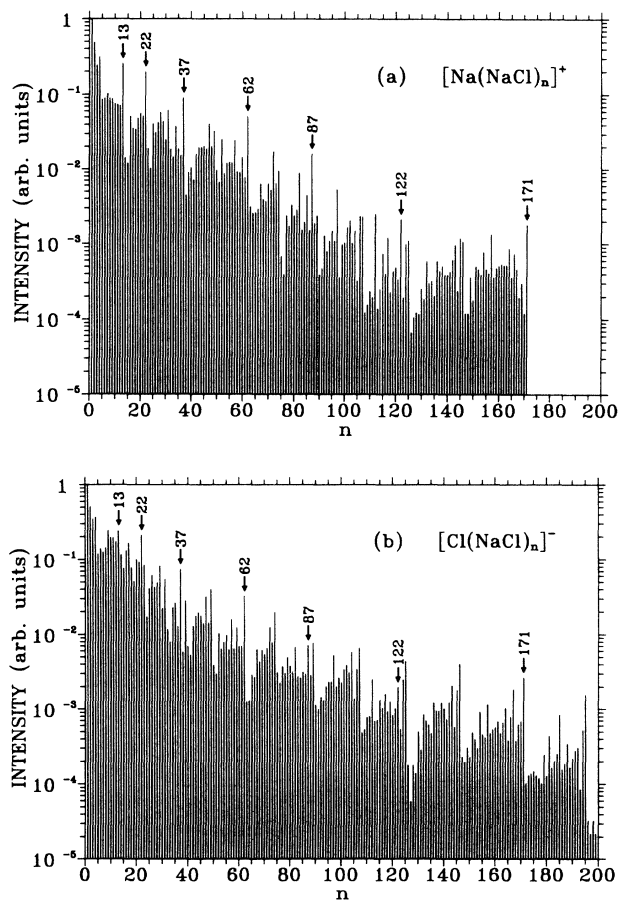


FIG. 4. Mass spectra of (a) positive and (b) negative NaCl cluster ions, obtained by integrating the total charge detected at each mass. The uncertainty for each point is  $\pm 10\%$ . For distant comparisons, there is an additional uncertainty of  $\pm 2\%$  to the power  $\Delta n$ .

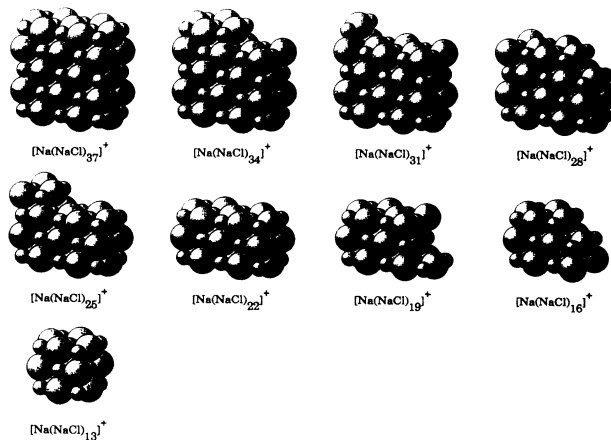


FIG. 5. The cuboid and cuboid plus terrace structures for sodium chloride positive cluster ions between  $\text{Na}(\text{NaCl})_{37}^+$  and  $\text{Na}(\text{NaCl})_{13}^+$ . Beginning with  $\text{Na}(\text{NaCl})_{37}^+$ , each new cluster ion is formed by removing a complete row of three NaCl molecules from the previous cluster ion. The geometries are approximate.

tems is almost purely ionic in character. The principal site for growth or decay in an ionic fcc crystal is at a kink site, shown in Fig. 6, where an incomplete row of ions is situated beside a complete terrace of ions on one side.<sup>18,19</sup> In an ionic fcc crystal, the last ion in the incomplete row is the easiest ion in the crystal to remove and the empty site next to it is the most attractive site for the addition of a new ion. During the high-temperature decay process, rows are peeled away at the kink sites so that once the first atom in a row is removed, the rest of the row evaporates easily. This process explains the surface terraces observed in the experiments.

Because the NaCl clusters follow this behavior, they appear to be relatively ionic in their bonding character. If a significant amount of covalent character were present, binding contributions from next-nearest neighbors would make the kink site ions more tightly bound than corner or edge ions. Then one would expect to see rounded corners on the clusters and a reduced importance of the kink sites in the growth and decay mecha-

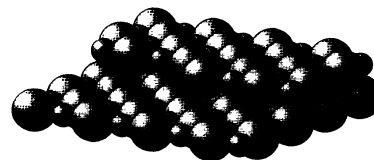


FIG. 6. The surface of bulk NaCl. The heavily outlined  $\text{Cl}^-$  ion is the "kink"-site ion, the end of an incomplete row of a surface terrace. It is the most easily removed ion from an ionic solid and its empty neighboring site presents the strongest attraction for an additional ion (see Ref. 18).

nisms.<sup>18</sup> The presence of such strong ionic character in the binding of these salt clusters is interesting because most of the atoms in each cluster are on the surface, where the Madelung energies are substantially reduced from those in the bulk solid. One might expect some amount of covalent bonding to appear at the surfaces.

For small clusters of alkali halides, it has been observed that stacked hexagonal rings of six ions per ring should be very stable neutral clusters.<sup>16,20</sup> A charged cluster with an additional ion attached to one end of this cylinder should also be unusually stable. In fact, the populations of clusters at  $n = 6$  and  $9$  are slightly increased in the negative-ion spectrum although they are not significantly larger than their neighbors in the positive-ion spectrum.

Unfortunately, some of the observed cluster ions formed and cooled as neutral species but then acquired charges through electron capture, charge exchange, or photoionization. In each of these cases, the charge change neutralized an ion, which subsequently evaporated from the cluster. Thus some clusters which started as  $\text{NaCl}(\text{NaCl})_n$  are observed as  $\text{Cl}(\text{NaCl})_n^-$  or  $\text{Na}(\text{NaCl})_n^+$  in the spectra. Particularly abundant among such clusters are those that began as neutral cuboids and then changed charge and lost a neutral atom. Some of these neutral cuboid-1 clusters are listed in Table I and can be found as abundant species in the cluster spectra, particularly among the negative cluster ions.

Cuboid cluster ions, cuboid ions with complete surface terraces, and neutral cuboid-1 ions account for the vast majority of abundance peaks in the spectra, both positive and negative. There are, however, a number of abundant species that cannot be explained by any of these three types of clusters. For positive clusters ( $n = 1-171$ ), the anomalous peaks are  $n = 60, 70, 85, 95, 106, 120, 145, 151, 154,$  and  $169$ . For negative cluster ions ( $n = 1-200$ ), they are  $n = 85, 106, 145, 151, 154,$  and  $194$ .

### B. Alkali-halide clusters

In addition to the spectra of  $\text{Na}(\text{NaCl})_n^+$  ( $n = 1-171$ ) and  $\text{Cl}(\text{NaCl})_n^-$  ( $n = 1-200$ ) shown in Fig. 4, we have measured the mass spectra for  $\text{Na}(\text{NaI})_n^+$  ( $n = 1-108$ ) and  $\text{I}(\text{NaI})_n^-$  ( $n = 1-125$ ), for  $\text{Cs}(\text{CsCl})_n^+$  ( $n = 1-125$ ) and  $\text{Cl}(\text{CsCl})_n^-$  ( $n = 1-125$ ), and for  $\text{Cs}(\text{CsI})_n^+$  ( $n = 1-100$ ) and  $\text{I}(\text{CsI})_n^-$  ( $n = 1-100$ ). These pairs of spectra appear in Figs. 7, 8, and 9 respectively. We have also looked at the spectra for potassium chloride  $\text{K}(\text{KCl})_n^+$  ( $n = 1-171$ ) and  $\text{Cl}(\text{KCl})_n^-$  ( $n = 1-171$ ) but have not included the results due to their similarity with NaCl clusters. All of these materials form cuboid fcc lattices, regardless of their bulk crystalline structure. Bulk sodium chloride, sodium iodide, and potassium chloride crystallize into the sixfold-coordinated fcc structure, while cesium chloride and cesium iodide prefer an eightfold-coordinated bcc lattice structure at normal pressures and temperatures. In fact, except for some features of the negative sodium iodide spectrum, cluster mass spectra of all these alkali halides have the same principal "magic numbers"—4, 13, 22, 37, 62, 87, and 122—and thus similar structures. Furthermore, the hex-

agonal ring structure peaks at  $n = 6$  and  $9$  are also present in all of these spectra. Cesium chloride and cesium iodide clusters do not have strong peaks at  $n = 7$ , in which 15 single ions can be arranged to form a bcc cube. The absence of a strong  $n = 7$  bcc cube peak and the presence of those strong fcc cuboid peaks indicate that the initial CsCl and CsI crystal growth is in the simple cubic form. This is consistent with a postulate by Martin that only after the crystal exceeds some critical size will a phase transition occur and the structure of the crystal change from simple cubic to bcc lattice.<sup>21</sup>

With the exception of sodium iodide negative cluster ions, almost all the peaks in these spectra can be explained as either cuboid clusters, surface terrace fine structure, small hexagonal rings, or neutral clusters that changed charge and lost an atom. However, unexplained peaks do appear for  $\text{Cs}(\text{CsI})_{18}^+$ ,  $\text{Cs}(\text{CsI})_{30}^+$ , and  $\text{Na}(\text{NaI})_{84}^+$ , along with the same unexplained peaks as seen in the NaCl cluster spectra:  $n = 60, 70, 85,$  and  $95$ .

Despite their general similarity, the spectra for different alkali halides and charge states are not identical. They differ in the amount of contrast between the popula-

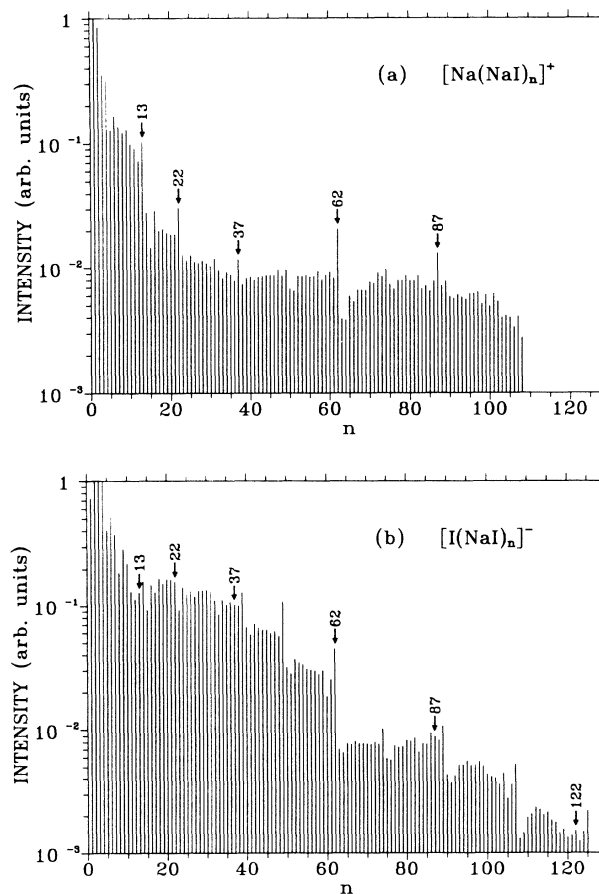


FIG. 7. Mass spectra of (a) positive and (b) negative NaI cluster ions.

TABLE I. Ion-abundance peaks at several  $n$  values result when neutral cuboid clusters of the form  $\text{NaCl}(\text{NaCl})_n$  become charged and lose an atom to become either  $\text{Na}(\text{NaCl})_n^+$  or  $\text{Cl}(\text{NaCl})_n^-$ . This table lists the cluster ions  $n$  that result from the most common neutral cuboid formats.

$n$	Format	$n$	Format	$n$	Format	$n$	Format
17	$3 \times 3 \times 4$	47	$4 \times 4 \times 6$	97	$4 \times 7 \times 7$	146	$6 \times 7 \times 7$
23	$3 \times 4 \times 4$	49	$4 \times 5 \times 5$	99	$5 \times 5 \times 8$	149	$5 \times 6 \times 10$
26	$3 \times 3 \times 6$	55	$4 \times 4 \times 7$	104	$5 \times 6 \times 7$	161	$6 \times 6 \times 9$
29	$3 \times 4 \times 5$	59	$4 \times 5 \times 6$	107	$6 \times 6 \times 6$	167	$6 \times 7 \times 8$
31	$4 \times 4 \times 4$	69	$4 \times 5 \times 7$	119	$5 \times 6 \times 8$	179	$5 \times 8 \times 9$
35	$3 \times 4 \times 6$	74	$5 \times 5 \times 6$	124	$5 \times 5 \times 10$	179	$6 \times 6 \times 10$
39	$4 \times 4 \times 5$	79	$4 \times 5 \times 8$	125	$6 \times 6 \times 7$	188	$6 \times 7 \times 9$
44	$3 \times 5 \times 6$	89	$5 \times 5 \times 6$	143	$6 \times 6 \times 8$	195	$7 \times 7 \times 8$

tions of cuboid clusters and adjacent cluster sizes. They also differ in the relative strengths of their fine structure. The differences in contrast we attribute to the lattice energies of alkali halides involved and the differences in fine structures appear to involve the relative sizes of the ions making up the clusters.

The light alkali halides have higher lattice energies than the heavy systems and also have substantially more contrast in their cluster spectra. For the four systems reported here, the lattice energies are as follows: NaCl, 7.92 eV/molecule; for NaI, 7.08 eV/molecule; for CsCl, 6.82 eV/molecule; and for CsI, 6.23 eV/molecule. NaCl

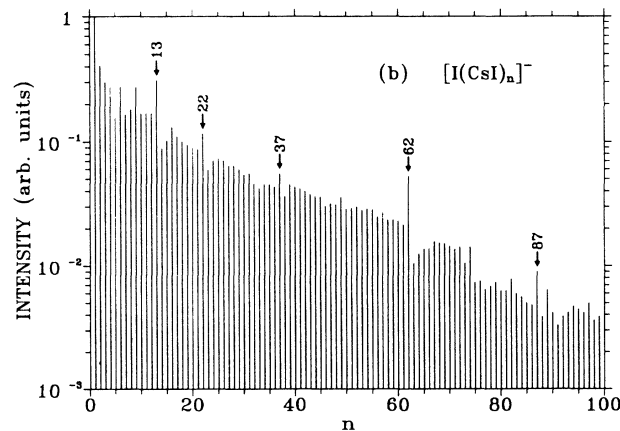
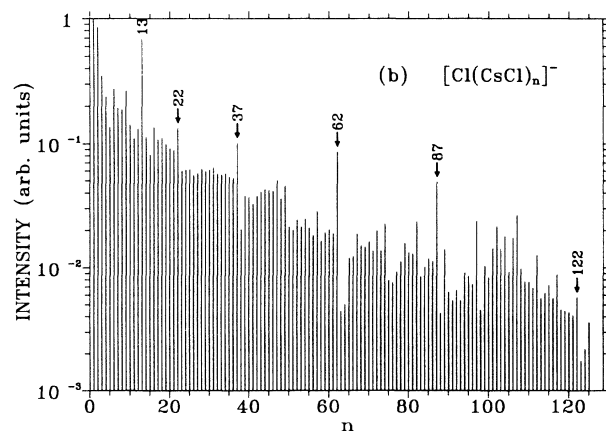
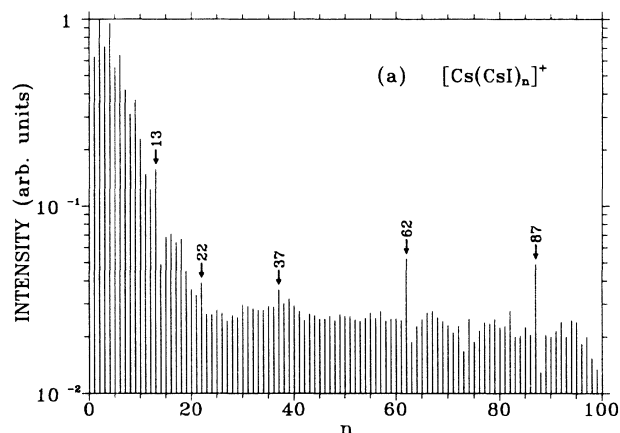
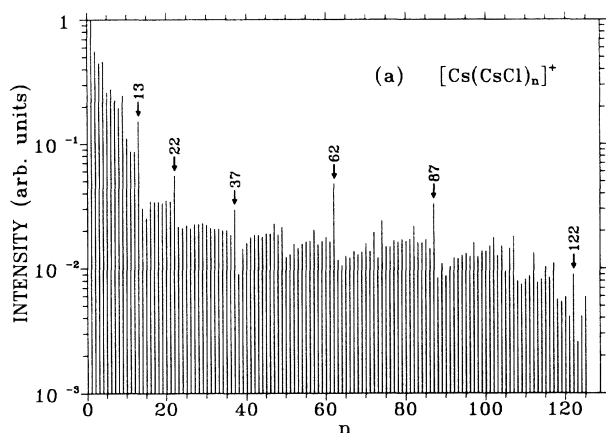


FIG. 8. Mass spectra of (a) positive and (b) negative CsCl cluster ions.

FIG. 9. Mass spectra of (a) positive and (b) negative CsI cluster ions.

exhibits the strongest contrast between the cuboid cluster ions and their neighboring cluster sizes, NaI and CsCl somewhat less, and finally CsI exhibits very little contrast. According to this principle, LiF, which has a very high lattice energy of 10.7 eV/molecule, should exhibit very high contrast between cuboid and noncuboid cluster ions. Unfortunately, we were essentially unable to produce cluster ions of LiF. A similar dependence of contrast on lattice spacing has been reported by Barlak, *et al.* in SIMS experiments on the alkali-halides.<sup>22</sup> In that work, they measure the abundance ratios of the "magic"  $n=4$  positive cluster ions ( $3 \times 3 \times 1$ ) to their non-"magic"  $n=3$  neighbors, for many different alkali halides. They find that the abundance ratio increases with decreasing lattice spacing (increasing lattice energy). Our present result, that contrast increases with lattice energy, is entirely consistent with that observation.

Because cations are generally smaller than anions, the crystal structure is determined primarily by the number of anions that can be packed around each cation and by the attractive and repulsive interactions between all of the ions. In an infinite lattice, an ionic material may choose between fcc and bcc lattices, depending on a delicate balance between attractive and repulsive contributions to the total energy. A bcc lattice has eight nearest neighbors, two more than fcc, and has both larger attractive and larger repulsive contributions to the total energy. The net energetic difference between fcc and bcc lattices is thus quite small. In a finite system, where a large amount of surface area is available to accommodate distortions, the material may be able to adopt a lattice structure other than fcc or bcc and further increase its bonding. Such distortions are particularly easy when the cation is extremely small compared to the anion, and can fill voids between the anions. Thus the ionic sizes of the con-

stituent ions of alkali halides affect not only the binding energies of the clusters, but the spatial arrangement of ions in those clusters as well.

The importance of the ion-size ratios to the structures of the clusters is immediately apparent in the spectrum of  $I(\text{NaI})_n^-$  cluster ions. The abundant cluster ions in this spectrum are quite different from those in any other spectrum. In particular, the cuboid enhancements at  $n=13$ , 22, 37, and 87 and the cuboid-1 structures at  $n=79$  and 97 disappear, the cuboid  $n=122$  is only a small peak, and some strange peaks such as  $n=14$ , 18, 24, 36, 93, and 98 are present. The absence of the  $n=13$  cuboid enhancement in the sodium iodide negative ion spectrum has also been observed in SIMS measurements.<sup>12,17</sup> In contrast, the spectrum for the  $\text{Na}(\text{NaI})_n^+$  clusters is essentially normal. We attribute this peculiar behavior to the dramatic size difference between the tiny  $\text{Na}^+$  and large  $\text{I}^-$  ions.

In the alkali-halide cluster sources used in this experiment, sodium iodide has the smallest free cation radius to free anion radius ratio. The cation radius  $R_M$  to anion radius  $R_X$  ratios are approximately

$$\begin{aligned} (R_{\text{Na}}/R_{\text{I}})_{\text{NaI}} (0.44) &< (R_{\text{Na}}/R_{\text{Cl}})_{\text{NaCl}} (0.54) \\ &< (R_{\text{K}}/R_{\text{Cl}})_{\text{KCl}} (0.74) \\ &< (R_{\text{Cs}}/R_{\text{I}})_{\text{CsI}} (0.76) \\ &< (R_{\text{Cs}}/R_{\text{Cl}})_{\text{CsCl}} (0.92) . \end{aligned}$$

Figure 10 is a juxtaposition of the  $n=51-69$  regions of the mass spectra for both the positive and negative alkali-halide cluster ions. The four compounds are displayed in order of their ion-size ratios, so that the left-most (sodium iodide) has the smallest ratio and the right-

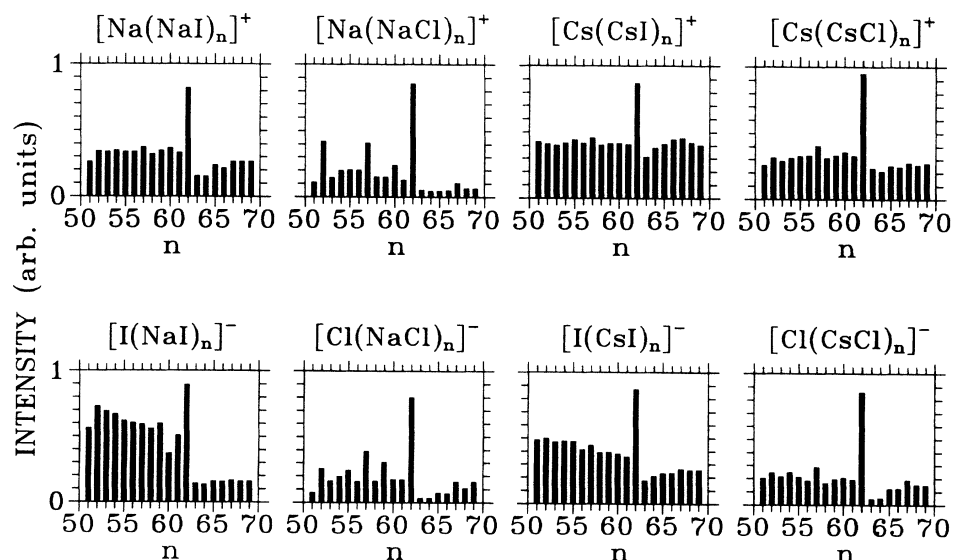


FIG. 10. Mass spectra for the alkali-halide cluster ions between  $n=50$  and  $n=70$ . The spectrum for NaI, with its small ion-size ratio, depends strongly on charge state, while the spectrum for CsCl, with nearly identical ion sizes, is independent of charge.

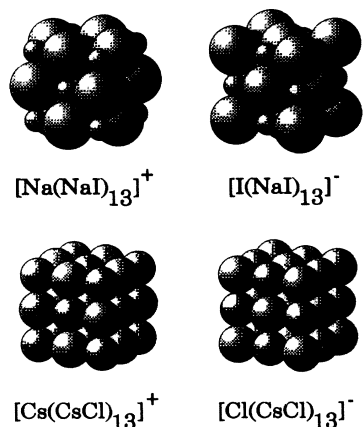


FIG. 11. The effects of ion-size ratio on cluster-ion geometry. Positive and negative cluster ions of sodium iodide NaI are very different, due to the large size difference between  $\text{Na}^+$  and  $\text{I}^-$ .  $\text{Cs}^+$  and  $\text{Cl}^-$  ions are almost indistinguishable in size. The geometries are approximate.

most (cesium chloride) has a ratio that is almost one. For cesium chloride, interchanging the negative and positive ions makes very little difference to the structure of each cluster because the ions have almost the same size (Fig. 11). In sodium iodide, the sodium ions are so much smaller than the iodine ions that the negative cluster ions are dramatically different from the positive cluster ions. This dependence of cluster structure on the relative sizes of its ions is reflected in the detailed structure of the cluster spectrum. In Fig. 10, we see that the abundance spectra of cesium chloride are insensitive to the charge states of the cluster ions because the two types of ions are nearly identical except for charge. But as the ions become less similar in size, a dependence on charge state begins to appear. For sodium iodide, the spectra are severely dependent on charge state.

#### IV. CONCLUSIONS

In the present study of alkali-halide clusters, the non-stoichiometric alkali-halide cluster ions  $M(MX)_n^+$  and

$X(MX)_n^-$  were produced by a laser-vaporization supersonic nozzle source and were measured by tilted-plate time-of-flight mass spectrometry. The source produces populations of cluster ions that reflect the relative high-temperature stabilities of those ions, although there are some ions present that formed as neutral clusters and then acquired a charge after cooling. The tilted-plate design of the spectrometer allows the measurements of very large molecular clusters. Mass spectra of NaCl, NaI, CsCl, and CsI cluster ions were obtained.

We find that, except for some features of the  $\text{I}(\text{NaI})_n^-$  spectrum, mass spectra of these alkali-halide cluster ions are surprisingly similar. The clusters tend to form fcc lattices, even though CsCl and CsI form bcc lattices at normal pressures and temperatures in the bulk. All of the clusters have the same fcc cuboid magic numbers: 13, 22, 37, 62, 87, and 122, surface terrace fine structure, and cuboid-1 enhancements that stem from charge changing processes. This implies that the initial CsCl and CsI crystal growth is in the simple cubic form. Furthermore, the spectra show that it is easier to see structures (i.e., there is better contrast) in the spectrum of the alkali halides with higher binding energies. Also, comparing the spectra of positive and negative clusters, we find that the relative stability of certain cluster ions is dependent upon the ionic radii of the constituents. The extraordinarily small cation to anion ion size ratio of 0.44, between the tiny  $\text{Na}^+$  ion and the large  $\text{I}^-$  ion, is probably responsible for the unique spectrum of  $\text{I}(\text{NaI})_n^-$  cluster ions. For CsCl, in which the  $\text{Cs}^+$  and  $\text{Cl}^-$  are almost the same size, the mass spectra show essentially no differences between positive and negative clusters.

#### ACKNOWLEDGMENTS

The authors gratefully acknowledge support from the National Science Foundation under Grant No. DMR-85-53312. Acknowledgment is also made to the donors of The Petroleum Research Fund, administered by the American Chemical Society, for partial support of this research.

- <sup>1</sup>K.-P. Huber and G. Herzberg, *Constants of Diatomic Molecules* (Van Nostrand/Reinhold, New York, 1979), p. 436.
- <sup>2</sup>C. Kittel, *Introduction to Solid State Physics*, 5th ed. (Wiley, New York, 1976), pp. 92 and 309.
- <sup>3</sup>J. E. Campana, T. M. Barlak, R. J. Colton, J. J. DeCorpo, J. R. Wyatt, and B. I. Dunlap, *Phys. Rev. Lett.* **47**, 1046 (1981).
- <sup>4</sup>R. Pflaum, P. Pfau, K. Sattler, and E. Recknagel, *Surf. Sci.* **156**, 165 (1985).
- <sup>5</sup>C. W. S. Conover, Y. A. Yang, and L. A. Bloomfield, *Phys. Rev. B* **38**, 3517 (1988).
- <sup>6</sup>R. Pflaum, K. Sattler, and E. Recknagel, *Chem. Phys. Lett.* **138**, 8 (1987).
- <sup>7</sup>C. W. S. Conover, Y. J. Twu, Y. A. Yang, and L. A. Bloomfield, *Rev. Sci. Instrum.* **60**, 1065 (1989).
- <sup>8</sup>J. B. Hopkins, P. R. R. Langridge-Smith, M. D. Morse, and R.

- E. Smalley, *J. Chem. Phys.* **78**, 1627 (1983).
- <sup>9</sup>Y. A. Lang and L. A. Bloomfield (unpublished).
- <sup>10</sup>B. P. Feuston, R. K. Kalia, and P. Vashishta, *Phys. Rev. B* **35**, 6222 (1987).
- <sup>11</sup>J. E. Campana, M. M. Ross, and J. H. Callahan, *Int. J. Mass Spectrom. Ion Phys.* **78**, 195 (1987).
- <sup>12</sup>J. E. Campana, R. J. Colton, J. R. Wyatt, R. H. Bateman, and B. N. Green, *Appl. Spectrosc.* **38**, 430 (1984).
- <sup>13</sup>H. Haberland, U. Buck, and M. Tolle, *Rev. Sci. Instrum.* **56**, 1712 (1985).
- <sup>14</sup>W. C. Wiley and I. H. McLaren, *Rev. Sci. Instrum.* **26**, 1150 (1951).
- <sup>15</sup>R. J. Beuhler, *J. Appl. Phys.* **54**, 4118 (1983).
- <sup>16</sup>T. M. Barlak, J. E. Campana, R. J. Colton, J. J. DeCorpo, and J. R. Wyatt, *J. Chem. Phys.* **85**, 3840 (1981).

- <sup>17</sup>J. E. Campana and B. I. Dunlap, *Int. J. Mass Spectrom. Ion Processes* **57**, 103 (1984).
- <sup>18</sup>J. W. Mitchell, *Photo. Sci. Eng.* **26**, 270 (1982).
- <sup>19</sup>M. H. Yang and C. P. Flynn, *Phys. Rev. Lett.* **62**, 2476 (1989).
- <sup>20</sup>T. P. Martin, *Phys. Rep.* **95**, 167 (1983).
- <sup>21</sup>T. P. Martin, *J. Chem. Phys.* **69**, 2036 (1978).
- <sup>22</sup>T. M. Barlak, J. E. Campana, J. R. Wyatt, and R. J. Colton, *J. Phys. Chem.* **87**, 3441 (1983).

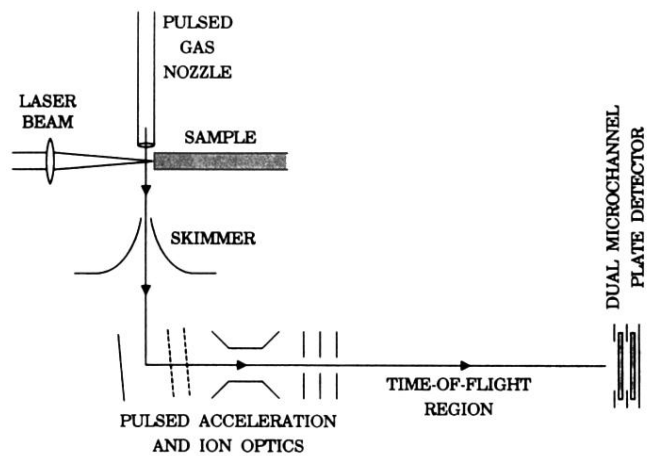


FIG. 1. Experimental apparatus: Cluster ions are produced by laser vaporization of the sample and are cooled and entrained in a helium-gas jet. The mass spectra of clusters produced in the source are obtained by tilted-plate time-of-flight mass spectrometry.

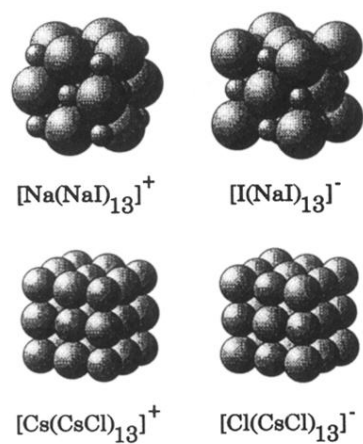


FIG. 11. The effects of ion-size ratio on cluster-ion geometry. Positive and negative cluster ions of sodium iodide NaI are very different, due to the large size difference between  $\text{Na}^+$  and  $\text{I}^-$ .  $\text{Cs}^+$  and  $\text{Cl}^-$  ions are almost indistinguishable in size. The geometries are approximate.

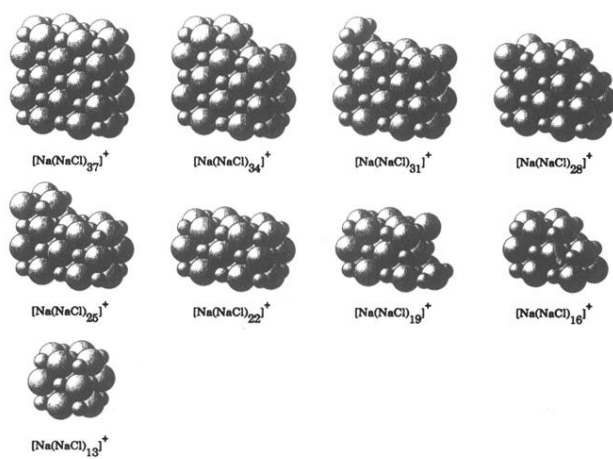


FIG. 5. The cuboid and cuboid plus terrace structures for sodium chloride positive cluster ions between  $\text{Na}(\text{NaCl})_{37}^+$  and  $\text{Na}(\text{NaCl})_{13}^+$ . Beginning with  $\text{Na}(\text{NaCl})_{37}^+$ , each new cluster ion is formed by removing a complete row of three NaCl molecules from the previous cluster ion. The geometries are approximate.

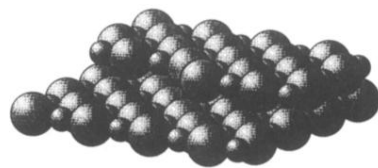


FIG. 6. The surface of bulk NaCl. The heavily outlined  $\text{Cl}^-$  ion is the "kink"-site ion, the end of an incomplete row of a surface terrace. It is the most easily removed ion from an ionic solid and its empty neighboring site presents the strongest attraction for an additional ion (see Ref. 18).